

RESEARCH ARTICLE

Stereoselective oxidation metabolism of 20(S)-protopanaxatriol in human liver microsomes and in rats

Wenyan Wang, Yingying Ni, Li Wang, Xin Che, Wanhui Liu, and Qingguo Meng

School of Pharmacy, Yantai University, Yantai, China

Abstract

1. In this study, the oxidative metabolites of 20(S)-protopanaxatriol (PPT) were identified in human liver microsomes (HLMs) and in rats using liquid chromatography-electrospray ionization tandem mass spectrometry.
2. Twelve oxidative metabolites were found in HLM, eight of which have not been previously reported. Twenty-four oxidative metabolites were found in rat feces after oral administration and 20 of these, including six found in HLM, were first reported. The results indicated PPT was more extensively metabolized in rats than in HLM. C20–24 epoxides, a pair of epimers (namely, M1-1 and M1-2) were the major metabolites, and other metabolites were derived from their further metabolism.
3. Enzyme kinetics experiments showed that the apparent formation V_{\max} of M1-1 was 10.4 folds and 2.4 folds higher than that of M1-2 in HLM and in rat liver microsomes (RLMs), respectively. The depletion rate of M1-2 was 11.0 folds faster than M1-1 in HLM, and was similar in RLM. Hence, the remarkable species differences of PPT metabolism mainly resulted from the stereoselective formation and further metabolic elimination of M1-1 and M1-2.
4. Chemical inhibition study and recombinant human P450 isoforms analysis showed that CYP3A4 was the predominant isoform involved in the oxidative metabolism of M1-1 and M1-2.

Keywords

20(S)-Protopanaxatriol, enzyme kinetics, liver microsomes, metabolite identification, P450 isoforms, stereoselectivity

History

Received 18 September 2014

Revised 7 November 2014

Accepted 7 November 2014

Published online 28 November 2014

Introduction

Ginsenosides content was 2–5% in ginseng roots and are known as the main active components of ginseng, having bioactive and pharmacological activities (Liu et al., 2010; Shibata, 2001). Furthermore, it has been reported that deglycosylation ginsenosides are more readily absorbed into the bloodstream and act as active components (Hasegawa et al., 1996; Lai et al., 2009; Sun et al., 2005; Tawab et al., 2003). 20(S)-protopanaxatriol (PPT; Figure 1) is a deglycosylation aglycone of the ginsenosides (such as Re, Rf, Rg1, Rg2 and Rh1) catalyzed by gastric acid and intestinal bacteria *in vivo* (Hasegawa, 2004; Liu et al., 2010). A number of studies have shown that PPT exhibits many pharmacological activities, including chemoprevention of cancer or inflammatory diseases (Oh et al., 2004), affecting the production of cortisol (Hasegawa et al., 2013) and anti-diabetic effect (Han et al., 2006), especially the antitumor effects (Chen et al., 2013; Hasegawa et al., 2002; Wang et al., 2009; Usami et al., 2008).

However, the absolute bioavailability of the PPT was estimated as 3.69% (Kong et al., 2013), which might result from its extensive metabolism in the liver. The study of the metabolic pathway of PPT has become very necessary to explore pharmacological potency and toxicology. Utilizing the NMR or MS analysis, many studies reported the microbial transformation products of PPT *in vitro* (Chen et al., 2013; Tian et al., 2005; Zhang et al., 2007) to investigate a possible biotransformation pathway *in vivo*. Kasai et al. (2000) have reported that PPT was metabolized to its C20–24 epoxides, by liver microsomes of rats *in vitro*. He et al. (2014) identified 22 metabolites of PPT in rats after oral administration, including its C20–24 epoxides. Wang et al. (2010) identified four metabolites of PPT after oral administration in mice, which were completely different from the metabolites in rats.

Furthermore, detecting and characterizing reactive metabolites in both experimental animals and humans is a highly important initial step to evaluate timely the hidden risks (Evans & Baillie, 2005), which can help to explore the species differences and extrapolate the results to humans. Han et al. (2011) reported PPT and one of its C20–24 epoxides exerted cardioprotective effects against myocardial ischemic injury, but another isoform had no effect. However, to the best of our knowledge, the metabolism information on PPT in humans is scant. In this study, the metabolism of PPT in mixed human

Address for correspondence: Wenyan Wang, School of Pharmacy, Yantai University, No 30 Qingquan Road, Laishan District, Yantai 264005, China. Tel: +86 535 6706030-8015. Fax: +86 535 6706066. E-mail: ytuwwy@163.com; Qingguo Meng, E-mail: qingguomeng@163.com

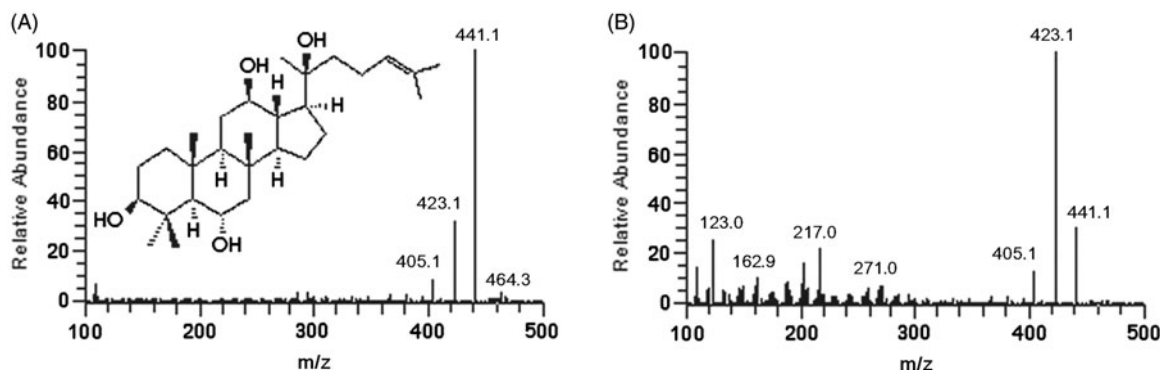


Figure 1. Chemical structure of PPT and its full scan mass spectrum (A) and MS² spectrum (B) in positive ionization modes from ESI source.

liver microsomes (HLMs) was examined. Meanwhile, the metabolites of PPT in rats after an oral administration were also identified to explore the species differences. The objectives of this study were as follows: (1) to characterize the structures of oxidative metabolites of PPT and compare the species differences; (2) to study the stereoselective formation and metabolic elimination of 20,24-epoxide epimeric metabolites of PPT; (3) to identify the cytochrome P450 (P450) enzymes responsible for the biotransformation of the epimeric metabolites.

Materials and methods

Chemicals and reagents

20(*S*)-Protopanaxatriol and schisandrin (internal standard, IS) with a purity of over 98% were provided by Chengdu Mansite Pharmaceutical Co., Ltd (Chengdu, China). Pooled HLMs (11 male Mongolian aged from 21 to 38 years) and Sprague–Dawley (SD) rat liver microsomes (RLM, 100 male SD rats aged from 2 to 3 months) were purchased from Rild Research Institute for Liver Diseases (Shanghai, China). β -Nicotinamide adenine dinucleotide phosphate, reduced form (NADPH) was purchased from Sigma-Aldrich (St. Louis, MO). Methoxsalen, quinidine and ketoconazole were purchased from J&K Scientific Co., Ltd (Beijing, China); and sulfaphenazole, ticlopidine, quercetin were purchased from China Food and Drug Inspection Institute (Beijing, China). cDNA-expressed human P450 isoforms (CYP1A2, CYP2C8, CYP2C9, CYP2C19, CYP2D6, CYP3A4 and CYP3A5) were purchased from BD Biosciences (San Jose, CA). Acetonitrile was of high-performance liquid chromatography (HPLC) grade (Merck KgaA, Darmstadt, Germany) and all other reagents were of analytical grade.

Incubations of PPT in human liver microsomes

A stock solution of PPT was prepared in acetonitrile. The final concentration of acetonitrile in the incubation was 0.5% (v/v). PPT (50 μ M) was incubated with the pooled HLM or RLM (1 mg/ml) in 100 mM phosphate buffer (pH 7.4) with 10 mM MgCl₂. The reaction volume was 200 μ l. After 3 min pre-incubation at 37 °C, the incubation reactions were initiated by the addition of NADPH (2.0 mM). Incubations were performed at 37 °C in a water bath shaker for 1 h. The reactions were terminated with an equal volume of ice-cold acetonitrile, and then stored at –20 °C until analysis. Control

samples without NADPH were included; each incubation was performed in duplicate. The incubations of the metabolites M1-1 (25 μ M) and M1-2 (25 μ M) in pooled HLM were carried out as described above for PPT, respectively.

Synthesis and identification of M1-1 and M1-2

m-CPBA (50 mg, 320 μ mol) was slowly added to the PPT solution (50 mg, 105 μ mol) in 25 ml of dichloromethane at room temperature. After stirring for 2 h, the reaction mixture was added to sodium carbonate-saturated ice water and extracted thrice with ethyl acetate. The organic extract was evaporated to dryness in a vacuum to obtain a residue. The residue was subjected to column chromatography on a C₁₈ reversed-phase silica gel and eluted with methanol:water (80:20) to produce M1-1 (21.6 mg) and M1-2 (19.2 mg). NMR spectra of M1-1 and M1-2 (¹H and ¹³C NMR, ¹H–¹H COSY, HSQC, HMBC and NOESY) were recorded on a Bruker Avance 400 spectrometer (400 MHz for ¹H and 100 MHz for ¹³C), and chemical shifts were recorded in parts per million using tetramethylsilane as an internal standard. Deuterium chloroform (CDCl₃) was used as a solvent.

Feces sample collection

SD male rats (239–264 g) were provided by the experimental animal center of Luye Pharma (Yantai, China). The animals were housed in standard cages in a light-controlled room at 19 ± 1 °C and 50 ± 5% relative humidity and given a standard pellet diet and water. All studies were conducted in accordance with the principles of Laboratory Animal Care (NIH publication no. 92–93, revised in 1985) and were approved by the local ethics committees for animal experimentation. The PPT was prepared as 10 mg/ml solution in 0.5% carboxymethyl cellulose sodium salt, 0.5% polysorbate-20. The solution was stirred at room temperature pending use. Five rats were housed in metabolic cages (one rat per cage) and given a single dose of PPT at 100 mg/kg by gavage. The feces samples were collected within a period of 0–48 h. The blank feces samples were collected prior to dosing. The feces samples were frozen at –20 °C immediately after collection.

Enzyme kinetics of M1-1 and M1-2 in RLM and HLM

Reaction mixtures containing pooled HLM or RLM (0.5 mg/ml) in 100 mM sodium phosphate buffer (pH 7.4) with 10 mM MgCl₂ were incubated at 37 °C in a water bath shaker. The

incubation volume was 200 μ l. The apparent formation kinetics of M1-1 and M1-2 were determined by incubating PPT at eight different concentrations (0.5, 1, 2, 5, 10, 20, 40 and 80 μ M) in RLM and HLM, respectively. After 3 min pre-incubation at 37 °C, the incubation reactions were initiated by the addition of NADPH (1.0 mM), and conducted at 37 °C for 15 min. The reactions were terminated with an equal volume of ice-cold acetonitrile and stored at -20 °C until analysis. The reaction velocity was linear with regard to both time and enzyme concentrations. Meanwhile, the depletion rates of this pair of epimers were determined after incubating M1-1 and M1-2 (0.5–40 μ M) in RLM and HLM, respectively. Control samples without NADPH were included. Each incubation was performed in triplicate. The reaction velocities were calculated in the unit of picomoles per minute per milligram of microsomal protein.

Microsomal incubations of M1-1 and M1-2 in the presence of inhibitors

Methoxsalen, quercetin, sulfaphenazole, ticlopidine, quinidine and ketoconazole were used as selective inhibitors of CYP1A2, CYP2C8, CYP2C9, CYP2C19, CYP2D6 and CYP3A, respectively. The inhibitors were dissolved in methanol, which was evaporated before incubation. The experiments were performed in pooled HLM (0.5 mg/ml) at 10 μ M M1-1 or M1-2 in the presence of each selective inhibitor at two different concentrations (1 and 10 μ M) in 100 mM phosphate buffer (pH 7.4) with 10 mM MgCl₂, respectively. The other conditions were same as above-mentioned enzyme kinetics experiments. For the mechanism-based inhibitor, methoxsalen was pre-incubated with all incubation constituents at 37 °C for 15 min before adding substrates, and ticlopidine was investigated with or without pre-incubation. The controls without the inhibitors or NADPH were included. Each incubation was performed in duplicate. The inhibitors were also incubated without any substrates under the same conditions to ensure that the inhibitors would not interfere with quantification of M1-1 and M1-2.

Metabolism of M1-1 and M1-2 in recombinant human P450 isoforms

M1-1 and M1-2, at 10 μ M concentrations, were incubated with human recombinant P450 isoforms (CYP1A2, CYP2C8, CYP2C9, CYP2C19, CYP2D6, CYP3A4 and CYP3A5) at 10 pmol in 100 mM phosphate buffer (pH 7.4) with 10 mM MgCl₂ and 1 mM NADPH, respectively. The reactions were initiated by adding the substrate, and carried out under the microsomal incubation conditions described in the enzyme kinetics experiments. The production of M2-3 and M2-4 were monitored by liquid chromatography tandem mass spectrometry (LC-MS/MS) and semi-quantitated according to the standard curves of M1-1 and M1-2, respectively.

Sample preparations for LC-MS/MS Analysis

All the *in vitro* incubation samples were prepared using the same methods. Methanol (400 μ l) was added to a 200 μ l incubation aliquot which had been terminated by acetonitrile, then vortex-mixed and centrifuged at 13 000 \times g for 10 min. The supernatant was transferred into a glass tube, evaporated

to dryness under a stream of nitrogen at 40 °C. The residue was reconstituted in 100 μ l of mixed solution of acetonitrile and water containing 0.1% formic acid (50:50, v/v). After grind and mixing, feces samples (0.2 g) was extracted by ultrasonic treatment with methanol for 30 min and then centrifuged at 13 000 \times g for 10 min. The following treatments were same as given above. A 20 μ l aliquot of the reconstituted solution was injected into the LC-MS/MS system for analysis.

LC-MS/MS conditions

LC-MS/MS was performed by an Agilent 1100 series HPLC system (Agilent Technologies, Waldbronn, Germany) and a TSQ Quantum Access tandem mass spectrometer (Thermo Electron Corporation, San Jose, CA) with an electrospray ionization (ESI) source. The analytes were separated with an XR-ODS C₁₈ column (50 mm \times 2.1 mm i.d., 2.2 μ m, Shimadzu, Japan). For the metabolite identification in HLM and in rat feces, the gradient elution was used to separate the metabolites with a mixture of A (acetonitrile) and B (water containing 0.1% formic acid) with the following procedures: 10% A for 0–2 min, 50% A for 5–8 min, 90% A for 10–13 min and 10% A for 14–20 min. A flow rate was 0.2 ml/min.

The mass spectrometer was operated in positive ionization mode. The spray voltage was 4 kV. Sheath gas and auxiliary gas pressures were 30 and 5 psi, respectively. The capillary temperature was 350 °C and argon gas pressure was 1.5 mTorr. Data acquisition was performed in full-scan of LC-MS and MS² modes. For MS spectra, the scan was ranged from *m/z* 100 to 1000, and the scan time was 0.8 s. For MS², the product ion spectra were produced via the collision-induced dissociation of the molecular ions [M + H]⁺ of all analytes at their respective HPLC retention times. All data obtained were processed using Xcalibur Workstation, version 1.4.1.

As for the quantitative analysis, the mobile phase was a combination of acetonitrile and water (containing 0.1% formic acid; 70:30, v/v) delivered at a flow rate of 0.2 ml/min. The selective reaction monitoring (SRM) in the positive ionization mode was applied to detect M1-1 and M1-2 (*m/z* 493.2 > 457.2) and IS (*m/z* 295.0 > 248.9) using the collision-induced decomposition voltages 20 and 28 eV, respectively. In addition, the dehydrogenation metabolites of the M1 were monitored semiquantitatively by SRM at *m/z* 491.2 > 455.2.

Data analysis

In enzyme kinetics experiments, the apparent kinetic parameters (V_{\max} and K_m) were calculated using Prism 5 (GraphPad Software, Inc., San Diego, CA) based on the Michaelis–Menten equation: $V = V_{\max} \cdot [S]/([S] + K_m)$, where K_m is the substrate concentration at half the maximum velocity (V_{\max}) of the reaction and $[S]$ is the substrate concentration.

Results

Identification the metabolites of PPT

Mass spectral properties of PPT

The full scan of the analytes in positive and negative ionization modes of the ESI source showed that the signals

obtained in positive ionization mode had sufficient abundance, which could be subjected to MS² analysis and provided more structural information. Due to the presence of four hydroxyl groups in the molecule, PPT is prone to generate in-source dissociation ions. Under the experimental conditions, the protonated molecule of PPT at m/z 477 was not detected, instead it was in-source dissociation ions at m/z 441 ($[M + H - 2H_2O]^+$) which further dehydrated in MS² to produce the fragment ions at m/z 423 ($[M + H - 3H_2O]^+$) and 405 ($[M + H - 4H_2O]^+$), as shown in Figure 1. The retention time of the PPT was at 15.4 min in the chromatography.

Identification metabolites of PPT in HLM

Compared with the control sample (without NADPH), 12 oxidation metabolites were found, including dehydrogenation, mono-oxidation, di-oxidation and tri-oxidation products. A series of extracting ion chromatograms of incubation samples of PPT, M1-1 and M1-2 in HLM are shown in Figure 2. By comparing the retention time and MS spectra with the incubation samples of M1-1 and M1-2 (the epimeric metabolites of PPT) in HLM, it could be inferred that other metabolites of PPT were produced by the sequential metabolism of M1-1 and M1-2. The structures were elucidated by their mass spectral fragmentation patterns (Figure 3).

Metabolite M1. As shown in Figure 2(A), M1-1 and M1-2 were detected at 12.8 and 14.6 min, respectively, with a protonated molecular weight of 493 (m/z 477 + 16), indicating the addition of one oxygen atom into the PPT molecule. The MS² spectra (Figure 3A) showed fragment ions at m/z 475 ($[M + H - H_2O]^+$), 457 ($[M + H - 2H_2O]^+$), 439 ($[M + H - 3H_2O]^+$) and 421 ($[M + H - 4H_2O]^+$). The latter two was 16 Da higher than the corresponding dehydrated ions of PPT, respectively. In addition, the fragment ions of m/z 143 and 207 were beneficial to identify the oxidation position. The standard references of M1-1 and M1-2 were synthesized chemically using *m*-CPBA. The data of NMR spectra were listed in Table 1, indicating that they were a pair of epimers, and that their difference lied only in the configuration at C24. By comparing the chromatographic retention time and mass spectral fragments with the synthesis metabolites (Figure 2A: e and f), M1-1 and M1-2 were confirmed as the (20*S*,24*S*)-epoxy-dammarane-3,6,12,25-tetrol and (20*S*,24*R*)-epoxy-dammarane-3,6,12,25-tetrol, respectively.

Metabolite M2. M2-1, M2-2, M2-3 and M2-4, with a quasi-molecular ion peak at m/z 491, were detected at 11.3, 13.2, 13.9 and 15.3 min, respectively. The MS² spectra (Figure 3B–D) showed identical fragment ions at m/z 473 ($[M + H - H_2O]^+$), 455 ($[M + H - 2H_2O]^+$), 437 ($[M + H - 3H_2O]^+$) and 419 ($[M + H - 4H_2O]^+$), which were 2 Da lower than the corresponding fragment ions of the M1. In addition, the fragment ions of m/z 143 and 205 were found in the MS² spectra of M2-2, which indicated the dehydrogenation occurring at C6. Only the fragment ion of m/z 143 was found in the MS² spectra of M2-3 and M2-4 that indicated the dehydrogenation occurring at C3. However, no inferential fragment ions were found at the low molecular weight region in the spectra of M2-1, so the dehydrogenation position of

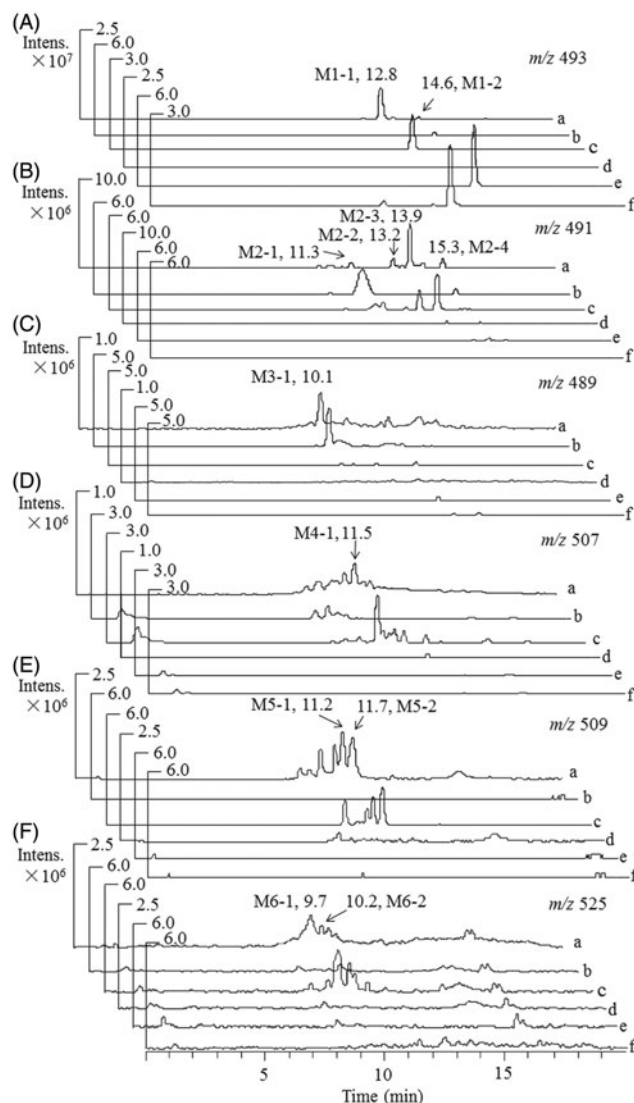


Figure 2. Extracted ion $[M + H]^+$ chromatograms of PPT metabolites after incubation PPT (50 μ M), M1-1 and M1-2 (25 μ M) with HLM. (A) M1 (m/z 493); (B) M2 (m/z 491); (C) M3 (m/z 489); (D) M4 (m/z 507); (E) M5 (m/z 509); (F) M6 (m/z 525). (a and d) PPT; (b and e) M1-2; (c and f) M1-1. (a, b and c), with NADPH. (d, e and f) without NADPH.

M2-1 was difficult to judge. By comparing the chromatographic retention time and mass spectral fragmentation patterns with the incubation sample of M1-1 and M1-2 (Figure 2B), it could be inferred M2-1 and M2-4 were the dehydrogenation metabolites of M1-2; M2-2 and M2-3 were the metabolites of M1-1.

Metabolite M3. M3-1 was detected at 10.1 min with a quasi-molecular ion peak at m/z 489. The MS² spectra (Figure 3E) showed the fragment ions at m/z 471 ($[M + H - H_2O]^+$), 453 ($[M + H - 2H_2O]^+$) and 435 ($[M + H - 3H_2O]^+$), which was 2 Da lower than the corresponding fragment ions of the M2. Due to the absence of the inferential fragment ions at the low molecular weight region, the dehydrogenation was speculated to be occurring at the bonds between the side chain and the host molecular moiety. Comparison of the chromatography and mass spectral characteristics with the incubation samples

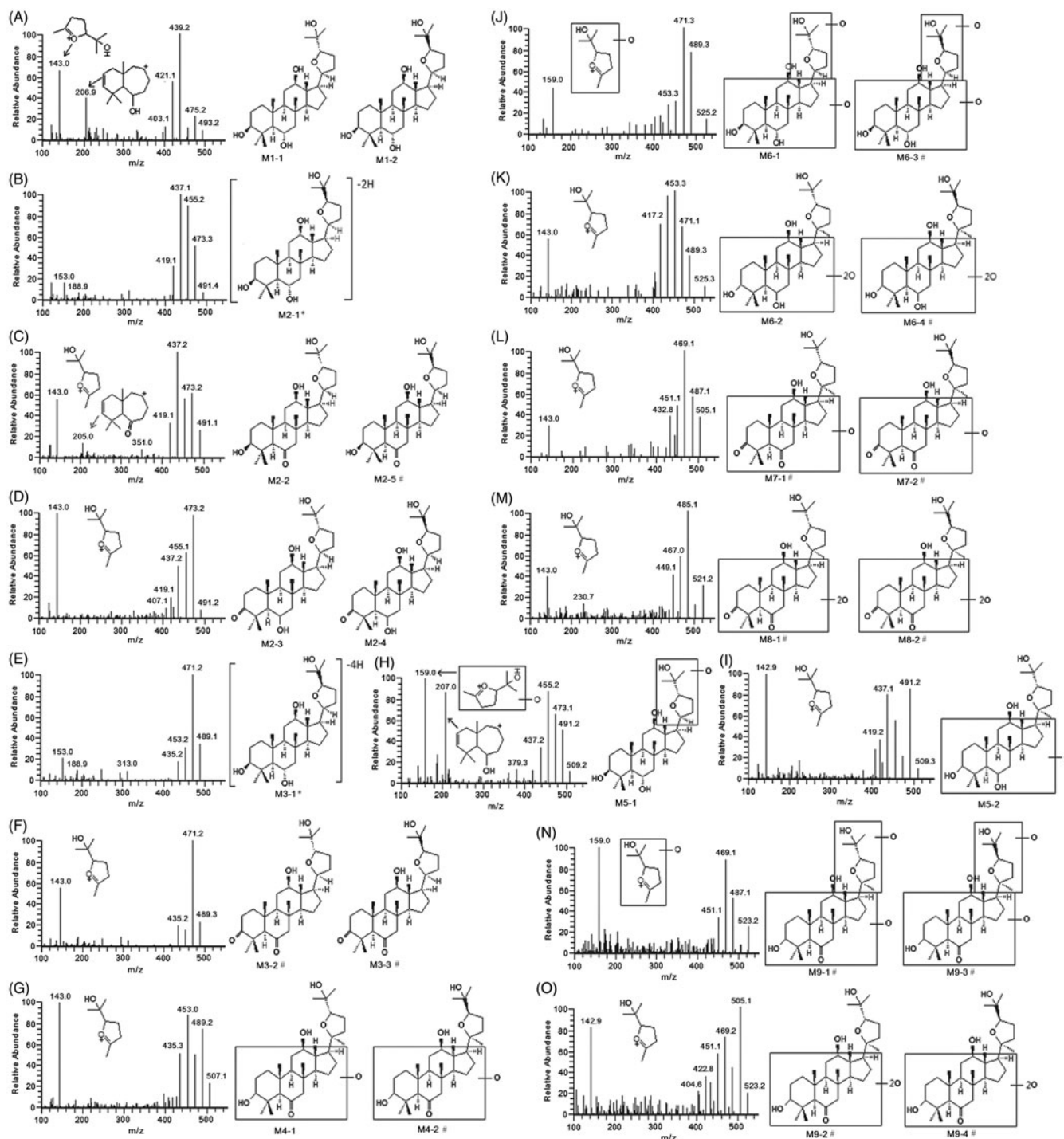


Figure 3. MS² spectra of PPT metabolites after incubation in HLM and oral administration to rats. (A) M1 (*m/z* 493); (B) M2-1* (*m/z* 491); (C) M2-2 and M2-5# (*m/z* 491); (D) M2-3 and M2-4 (*m/z* 491); (E) M3-1* (*m/z* 489); (F) M3-2# and M3-3# (*m/z* 489); (G) M4-1 and M4-2# (*m/z* 507); (H) M5-1 (*m/z* 509); (I) M5-2 (*m/z* 509); (J) M6-1 and M6-3# (*m/z* 525); (K) M6-2 and M6-4# (*m/z* 525); (L) M7# (*m/z* 505); (M) M8# (*m/z* 521); (N) and (O) M9# (*m/z* 523). * only found in HLM incubations; # only detected in rat feces.

of M1-1 and M1-2 (Figure 2C) indicated that M3-1 was the dehydrogenation metabolite of M1-2.

Metabolite M4. M4-1 was detected at 11.5 min with a quasi-molecular ion peak at *m/z* 507. The MS² spectra (Figure 3G) showed the fragment ions at *m/z* 489 ([M + H - H₂O]⁺), 471 ([M + H - 2H₂O]⁺), 453 ([M + H - 3H₂O]⁺) and 435 ([M + H - 4H₂O]⁺), which was 16 Da higher than the corresponding fragment ion of the M2. Presence of the fragment ion of *m/z*

143 suggested the occurrence of another oxidation modification on the host molecular moiety. Comparison of the chromatography and mass spectral characteristics with the metabolites of the M1 (Figure 2D) suggested that M4-1 was the further dehydrogenation and oxidation product of M1-1.

Metabolite M5. M5-1 and M5-2 were detected at 11.2 and 11.7 min, respectively, with a protonated molecular weight of

Table 1. NMR data for M1-1 and M1-2 in $CDCl_3$.

	M1-1				M1-2		
	δ_H (J in Hz)	δ_C	HMBC	NOESY	δ_H (J in Hz)	δ_C	NOESY
1	1.72, m; 1.05, m	38.62	2, 5		1.69, m; 1.03, m	38.67	
2	1.68, m; 1.59, m	26.96	1		1.66, m; 1.59, m	26.98	
3	3.18, dd (10.0, 4.3)	78.06	1, 28, 29	5, 28	3.17, dd (11.0, 3.8)	78.39	5, 28
4		39.20				39.21	
5	0.90, m	61.14	28, 29	3, 9	0.90, m	61.18	3, 9
6	4.12, td (10.6, 3.0)	68.56	5, 10		4.11, t (10.2)	68.53	
7	1.62, m; 1.52, m	46.79	5, 9, 10		1.63, m; 1.50, m	46.86	
8		40.79				40.78	
9	1.50, t (12.4)	49.59			1.49, m	49.88	
10		39.03				38.99	
11	1.94, m; 1.15, m	31.41	8		1.92, m; 1.07, m	31.13	
12	3.52, td (9.8, 4.3)	70.36	9, 14	9, 17, 30	3.51, td (10.2, 4.3)	70.80	9, 18
13	1.68, m	48.28	11, 17, 30		1.67, m	48.92	
14		51.90				51.76	
15	1.54, m; 1.12, m	32.12	13, 17		1.59, m; 1.41, m	32.55	
16	1.98, m; 1.32, m	28.45	13, 14		2.01, m; 1.32, m	28.52	
17	2.25, td (11.0, 3.0)	48.74	15, 20	9, 21, 30	2.19, t (9.4)	47.79	18, 21
18	1.09, s	16.91	7, 11, 14		1.06, s	16.84	
19	0.94, s	17.30	1, 5, 9, 10		0.90, s	17.37	
20		87.03				86.41	
21	1.27, s	28.78	17, 20, 22	17, 26	1.28, s	27.51	24
22	1.90, m; 1.78, m	31.56			1.85, m; 1.66, m	31.13	
23	2.05, m; 1.87, m	25.02	25		2.03, m; 1.88, m	24.90	
24	3.88, dd (10.2, 4.3)	87.36	25	27	3.85, t (7.7)	85.33	21, 27
25		70.05				70.09	
26	1.11, s	24.07	24	24	1.09, s	26.06	24
27	1.23, s	27.89	24	24	1.28, s	27.85	24
28	1.31, s	30.76	3, 4, 5	3, 5	1.31, s	30.76	3, 5
29	0.98, s	15.41	3, 4, 5		0.97, s	15.40	
30	0.94, s	17.66	8, 13, 15		0.93, s	18.07	

509 (m/z 477 + 32), indicating the introduction of two oxygen atoms into the PPT molecule. The MS^2 spectra (Figure 3H and I) showed the fragment ions at m/z 491 ($[M + H - H_2O]^+$), 473 ($[M + H - 2H_2O]^+$), 455 ($[M + H - 3H_2O]^+$) and 437 ($[M + H - 4H_2O]^+$), which was 16 Da higher than the corresponding fragment ions of the M1. The presence fragment ions of m/z 159 and 207 in M5-1 showed another oxidation happened in the side chain moiety of the M1, and the fragment ion of m/z 143 in M5-2 indicated another oxidation occurred on the host molecular moiety of the M1. In addition, by comparing spectra characteristics with the incubation sample of M1 (Figure 2E), it could be concluded M5 can be produced by the metabolism of M1-1.

Metabolite M6. M6-1 and M6-2 were detected at 9.7 and 10.2 min, respectively, with a protonated molecular weight of 525 (m/z 477 + 48), indicating the introduction of three oxygen atoms. The MS^2 spectra (Figure 3J and K) showed identical fragment ions at m/z 489 ($[M + H - 2H_2O]^+$), 471 ($[M + H - 3H_2O]^+$) and 453 ($[M + H - 4H_2O]^+$), which was 32 Da higher than the corresponding fragment ions of the M1. However, the presence fragment ion of m/z 159 and 143 in the MS^2 spectra of M5-1 and M5-2, respectively, indicated the third oxidation happening in the side chain moiety in M5-1 and the host molecular moiety in M5-2. In addition, comparison of chromatography and mass spectra profiles showed that M6-1 and M6-2 could be produced by the metabolism of M1-1 (Figure 2F).

Identification metabolites of PPT in rat feces

A series of extracting ion chromatograms of experimental feces samples are shown in Figure 4. After oral administration of PPT to rats, a total of 24 metabolites were detected in feces and tentatively identified. Excluding M1 and M5, whose structures were similar to M1 and M5 identified in HLM, other 20 metabolites were first reported according to the ocotillo-type structure. Among the 20 metabolites, 6 metabolites were consistent with those characterized in HLM: M2-2, M2-3, M2-4, M4-1, M6-1 and M6-2. Other 14 metabolites are described as follows.

Metabolite M2. M2-5 was detected at 14.2 min besides M2-2, M2-3 and M2-4, with a quasi-molecular ion peak at m/z 491. The MS^2 spectrum of M2-5 was identical with that of M2-2 derived from M1-1. According to the retention time, M2-5 was supposed to be produced by the sequential metabolism of M1-2.

Metabolite M3. M3-2 and M3-3 were detected at 13.0 and 14.9 min, respectively, with a quasi-molecular ion peak at m/z 489. The fragment ion of m/z 143 was found in their MS^2 spectra, which showed that the dehydrogenation occurred at the host molecular moiety (Figure 3F). According to the retention time, M3-2 and M3-3 were inferred as the further dehydrogenation metabolites of the M1.

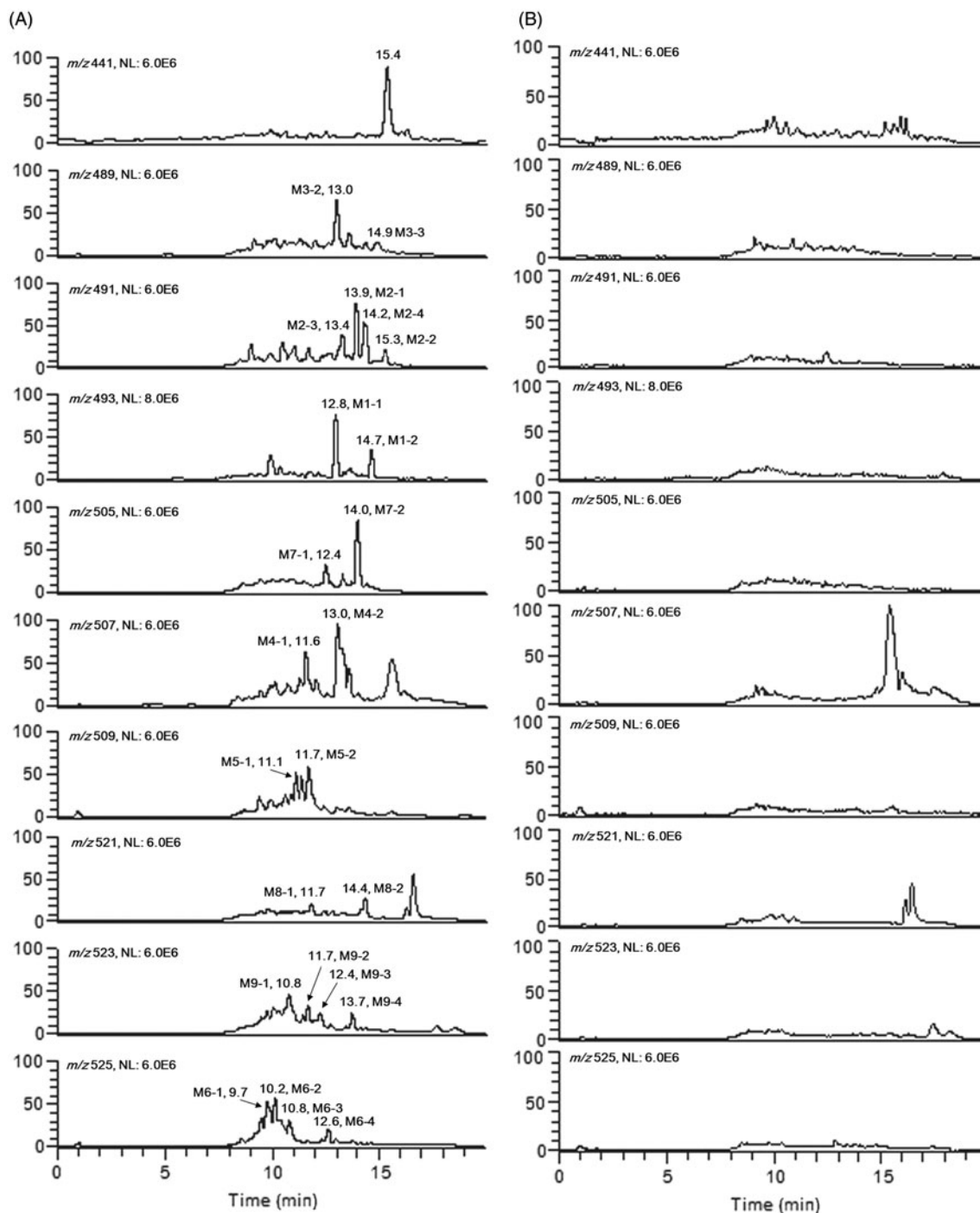


Figure 4. Extracted ion $[M+H]^+$ chromatograms of PPT metabolites in rat feces after oral administration of PPT. (A) The feces of 0–24h after administration and (B) the feces prior to administration.

Metabolite M4. M4-2 was detected at 13.0 min besides M4-1 at 11.6 min, with a quasi-molecular ion peak at m/z 507. Their MS^2 spectra were same. It has been inferred that M4-1 was the further dehydrogenation and oxidation product of M1-1 in HLM incubations. Therefore, it was supposed that M4-1 and M4-2 were the further metabolites of M1-1 and M1-2 in rats, respectively, according to the chromatography retention time.

Metabolite M6. M6-3 and M6-4 were detected at 10.8 and 12.6 min, respectively, besides M6-1 and M6-2 at 9.7 and

10.2 min, with a quasi-molecular ion peak at m/z 525. M6-1 and M6-2 had been identified as the further oxidation products of M1-1 in HLM incubations. The MS^2 spectrum of M6-3 and M6-4 was same as that of M6-1 and M6-2, respectively (Figure 3J and K). Hence, it was inferred that M6-1 and M6-2 were the further oxidation products of M1-1 in rats, and M6-3 and M6-4 were the metabolites of M1-2.

Metabolites M7. M7-1 and M7-2 were detected at 12.4 and 14.0 min, respectively, with a quasi-molecular ion peak at m/z 505. The MS^2 spectra (Figure 3L) showed the fragment ions

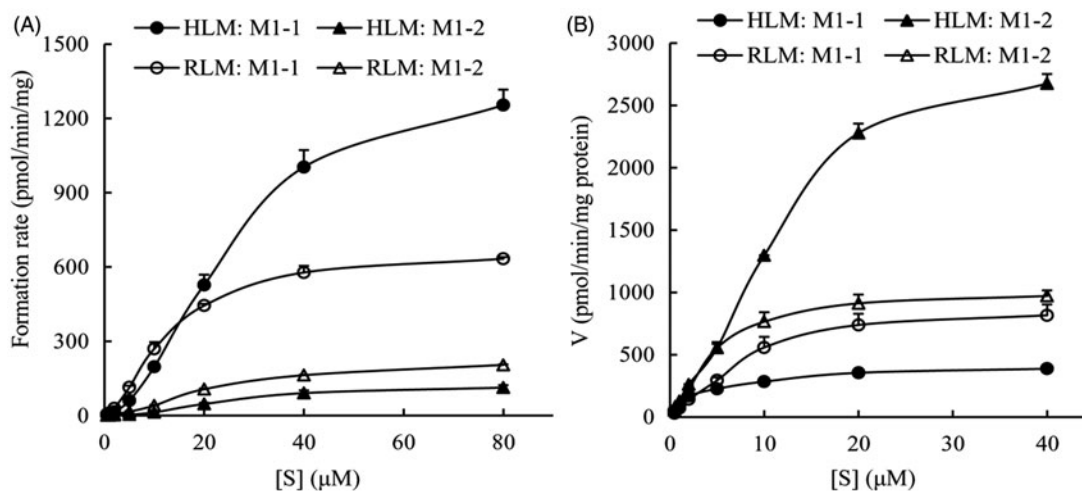


Figure 5. (A) Formation kinetic plots and (B) elimination kinetic plots of M1-1 and M1-2 in RLM and HLM. PPT (0.5–80 μM), M1-1 and M1-2 (0.5–40 μM) were, respectively, incubated with microsomes (0.5 mg/ml) containing 1 mM NADPH for 15 min at 37 $^{\circ}\text{C}$. Data are expressed as the mean values of three separate determinations.

at m/z 487 ($[\text{M} + \text{H} - \text{H}_2\text{O}]^+$), 469 ($[\text{M} + \text{H} - 2\text{H}_2\text{O}]^+$), 451 ($[\text{M} + \text{H} - 3\text{H}_2\text{O}]^+$) and 433 ($[\text{M} + \text{H} - 4\text{H}_2\text{O}]^+$), which was 16 Da higher than the corresponding fragment ions of the M3. In addition, the fragment ion m/z 143 was found, so it was presumed another oxidation modification occurred on the host molecular moiety.

Metabolite M8. M8-1 and M8-2 were detected at 11.7 and 14.4 min, respectively, with a quasi-molecular ion peak at m/z 521. The MS^2 spectra (Figure 3M) showed the fragment ions at m/z 503 ($[\text{M} + \text{H} - \text{H}_2\text{O}]^+$), 485 ($[\text{M} + \text{H} - 2\text{H}_2\text{O}]^+$), 467 ($[\text{M} + \text{H} - 3\text{H}_2\text{O}]^+$) and 449 ($[\text{M} + \text{H} - 4\text{H}_2\text{O}]^+$), which was 16 Da higher than the corresponding fragment ions of the M7. In addition, the fragment ion m/z 143 was present, so it was presumed the third oxidation happened at the host molecular moiety.

Metabolite M9. M9-1, M9-2, M9-3 and M9-4 were detected at 10.8, 11.7, 12.4 and 13.7 min, respectively, with a quasi-molecular ion peak at m/z 523. The MS^2 spectra (Figure 3N and O) showed identical fragment ions at m/z 505 ($[\text{M} + \text{H} - \text{H}_2\text{O}]^+$), 487 ($[\text{M} + \text{H} - 2\text{H}_2\text{O}]^+$), 469 ($[\text{M} + \text{H} - 3\text{H}_2\text{O}]^+$) and 451 ($[\text{M} + \text{H} - 4\text{H}_2\text{O}]^+$), which was 16 Da higher than the corresponding fragment ions of the M4. In addition, the fragment ion of m/z 159 was found in MS^2 spectra of M9-1 and M9-3, so it was presumed the third oxidation happened at the side chain moiety. Similarly, the ion of m/z 143 was found in M9-2 and M9-4, so it was presumed the third oxidation happened in the host molecular moiety.

Stereoselective formation and metabolism of M1-1 and M1-2 in HLM and RLM

As shown in Figure 5(A), the apparent formation rate of M1-1 was higher than that of M1-2 when incubating PPT with RLM and HLM. The V_{max} of M1-1 was 2.4 folds and 10.4 folds higher than that of M1-2 in RLM and HLM, respectively (Table 2).

The average depletion rates of M1-1 and M1-2 were estimated from the differences between the zero time point

and the time point after 15 min incubation. The metabolic elimination profiles are shown in Figure 5(B), the depletion rate of M1-2 was 11.0 folds faster than that of M1-1 in HLM, and the depletion rate of M1-1 and M1-2 was similar in RLM (Table 2). The results indicated that there were stereoselective differences and species differences in the formation and metabolic elimination between M1-1 and M1-2.

Identification of P450 enzymes responsible for M1-1 and M1-2 metabolism

After the incubation of M1-1 and M1-2 (10 μM) with six types of inhibitors of microsomal P450 isoform enzymes (CYP1A2, CYP2C8, CYP2C19, CYP2C9, CYP2D6 and CYP3A) in HLM, the inhibition data were expressed as relative activity compared with the control incubations without inhibitors or NADPH. Among the inhibitors used, only ketoconazole showed a significant inhibitory effect on the oxidative metabolism of M1-1 and M1-2, yielding about 95% inhibition at 10 μM (Figure 6), whereas other isoform enzyme inhibitors had no inhibitory effects on their metabolism essentially.

In seven types of recombinant human P450 isoforms tested, as expected, only CYP3A4 and CYP3A5 at a minor extent (less than 5% that of CYP3A4) exerted catalytic activity for M1-1 and M1-2, meanwhile the dehydrogenation metabolites of M1-1 and M1-2 were detectable. The catalytic activity of other isoforms tested to M1-1 and M1-2 was negligible. These data showed that CYP3A4 was probably the major isoform enzyme responsible for the further oxidative metabolism of M1-1 and M1-2.

Discussion

Both negative and positive modes of ESI mass spectra were examined in this study. Generally, in the negative mode, fewer product ions were observed in quadrupole mass analyzer; while in the positive ion mode, $[\text{M} + \text{H}]^+$ ions with sufficient abundance were subjected to MS^2 analysis and provided more structural information. Proper metabolite identification using

Table 2. Enzyme kinetic parameters of formation or metabolic elimination for M1-1 and M1-2, the epimeric metabolites of PPT, in RLM and HLM.

	Formation		Elimination	
	V_{max} (pmol/min/mg protein)	K_m (μ M)	V_{max} (pmol/min/mg protein)	K_m (μ M)
RLM				
M1-1	844.5 \pm 62.0 ^a	21.6 \pm 1.8	1089 \pm 80.4	11.2 \pm 1.1
M1-2	354.9 \pm 34.5	54.1 \pm 4.6	1173 \pm 68.6	6.3 \pm 0.7
HLM				
M1-1	2593 \pm 125 ^b	78.8 \pm 5.7	411.7 \pm 15.1	3.6 \pm 0.47
M1-2	249.3 \pm 31.0	88.9 \pm 7.8	4539 \pm 308 ^c	25.0 \pm 2.6

The maximum velocity (V_{max}) and the Michaelis constant (K_m , the substrate concentration at half V_{max}) were estimated from the Michaelis–Menten equation by non-linear regression analysis of the mean values of three separate determinations.

^a p < 0.01 versus M1-2 in RLM.

^b p < 0.01 versus M1-2 in HLM.

^c p < 0.01 versus M1-1 in HLM.

the LC-MS/MS approach requires a comprehensive understanding of the fragmentation behavior of the compound to be tested. In this study, a total of 12 oxidation metabolites were found in HLM incubations and 24 oxidation metabolites were found in rat feces by LC-MS/MS methods. It suggested that there were more extensive oxidation metabolism in rats than in humans. In order to demonstrate whether there were other metabolic pathways besides the hepatic metabolism, the metabolism study of PPT in RLM was also carried out. Since the results were similar to that in rat feces, the data are not shown here.

In order to explain the extensive pharmacological activities of PPT and explore the toxicological potency, the metabolic pathway study of PPT has been undertaken *in vitro* and *in vivo*. Microbial biotransformation studies showed that PPT mainly yielded the compounds of dehydrogenation at C12 or hydroxylation at C15, C26, C27, C28, C29 and 20S,24R-epoxy-dammaran-3 β ,6 α ,25-triol-12-one by the fungus *Mucor spinosus* or *Absidia corymbifera* AS (Chen et al., 2013; Tian et al., 2005; Zhang et al., 2007). Wang et al. (2010) revealed one phase I intestine metabolite of PPT in mice. PPT carried out dehydrogenation at C12 and hydroxylation at C15, as well as formation of an ester bond at C20 of the side chain. In a recent research report (He et al., 2014), 17 phase I metabolites were found in rats, and it was proposed that the predominant metabolic pathways of PPT were oxidation to yield two of C20–24 epoxides, i.e. M1-1 and M1-2 in our study; and form corresponding carboxylic acid at C26/27. Hao et al. (2010) proposed that the formation of C20–24 epoxides (ocotillol-type ginsenosides) were the main oxygenation metabolism pathway of PPT-type ginsenosides by microsomal P450-mediated. In this study, by comparing the chromatographic retention times and mass spectral fragments of incubation samples of PPT with those of M1-1 and M1-2 in HLM, it was probable to infer the further oxidative metabolites were produced by sequential metabolism of M1-1 and M1-2. The proposed metabolic pathways of PPT were different from the previous report. Moreover, earlier studies (Li et al., 2011, 2012) found that the predominant metabolic pathway of 20(S)-protopanaxatriol (PPD) and 20(S)-ginsenoside Rh2 in HLM was the oxidation that yielded the 20,24-epoxide form. The further sequential metabolites were also detected through

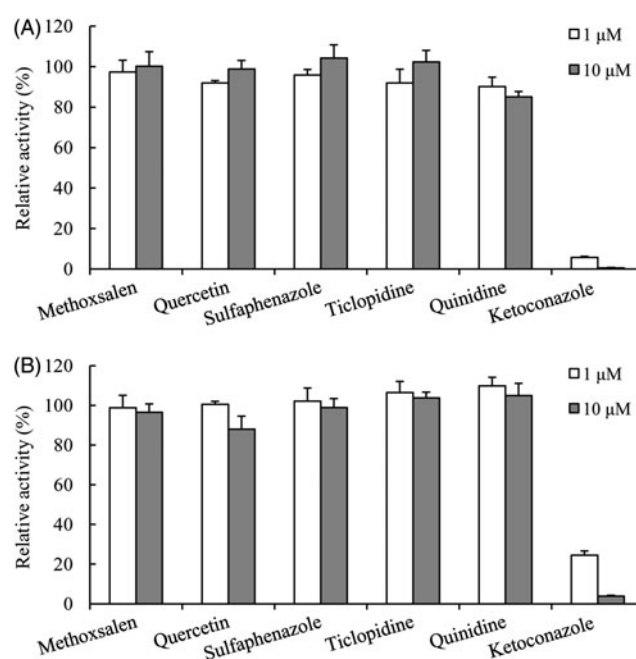


Figure 6. Effects of isoform-selective P450 inhibitors on the metabolism of M1-1 (A) and M1-2 (B) in incubation with HLM. Reactions were performed in the presence of M1-1 or M1-2 (10 μ M) with different isoform enzyme inhibitors at two concentrations (1.0 and 10 μ M) in the microsomes (0.5 mg/ml) containing 1 mM NADPH at 37 °C for 15 min. Data are reported as the mean values of two separate determinations.

the dehydrogenation and/or oxygenation of the C20–24 epoxides. Hence, C20–24 epoxides were important intermediate metabolites of PPT in HLM and its further dehydrogenation metabolite with higher abundance (Figure 2), which was aid to support the further active compounds and toxicological studies.

Compared with HLM, oxidation metabolites were found more in rat feces samples. In addition, this study showed that the apparent formation quantity of M1-1 was far more than that of M1-2 after the incubation of PPT in HLM. As P450 enzymes are important in the metabolism of xenobiotics and are highly stereoselective (Li et al., 2005; Shimshoni et al., 2012; Sun et al., 2013), many chiral compounds are produced

by the metabolism. The further kinetic studies in the apparent formation and metabolic elimination of M1-1 and M1-2 in HLM and in RLM discovered the formation V_{\max} of M1-1 was 10.4 folds higher than that of M1-2, and the depletion rate of M1-2 was 11.0 folds faster than M1-1 in HLMs. The apparent formation differences between M1-1 and M1-2 might ascribe to the fast depletion rate of M1-2. However, the apparent formation V_{\max} of M1-1 was 2.4 folds higher than that of M1-2, and the depletion rates of M1-1 and M1-2 were similar in RLM. This indicated there were remarkable stereoselectivity differences in the elimination and formation between M1-1 and M1-2. The elimination difference was mainly manifested in HLM incubation, and the formation difference was confirmative in RLM. Obviously, the stereoselectivity metabolism of both epimers had species differences between rats and humans. It suggests that besides the differences in isoform composition, expression and catalytic activities of drug-metabolizing enzymes across species, the stereoselectivity difference was also important between species. In addition, stereochemistry is an important dimension in pharmacology and it often results in different pharmacological activities of chiral xenobiotics. The pharmacological activity study of PPT and its epimeric metabolites showed that PPT and M1-2 exerted cardioprotective effects against myocardial ischemic injury by enhancing the anti-free-radical actions of heart tissues, and M1-1 had no such effect (Han et al., 2011). This study suggested that M1-1, 24S-epimer was the predominant metabolite of PPT in clinical situations.

It has been well known that CYP3A is the most abundant human hepatic P450 isoforms and accounts for the metabolism of approximately 50% of drugs in clinical use. Hao et al. (2010) found CYP3A4 mediated oxygenation metabolism of PPT type ginsenosides and the metabolites of C20–24 epoxides (M1 and M5) were produced. The studies (Chiu et al., 2014; Li et al., 2012) demonstrated that CYP3A was the sole isoform involved in the oxygenation metabolism of ginsenosides Rh2 and PPD, and compared with CYP3A5, CYP3A4 should be the predominant isoform. Both chemical inhibition and recombinant human P450 isoform assays in the present study indicated that CYP3A4 was the predominant isoform responsible for the further oxidation metabolism of M1-1 and M1-2. Potential drug–drug interaction should be kept in mind when drugs influencing CYP3A4 activity or being substrates of CYP3A are co-administered with PPT.

Conclusion

In this study, 12 and 24 oxidation metabolites of PPT were found in HLM and rats, respectively. C20–24 epoxides, M1-1 and M1-2 were the major metabolites. Moreover, other metabolites were inferred from the sequential metabolism of the M1 by comparing ESI-MS/MS spectra and chromatography characteristics. PPT underwent more extensive oxidative metabolism in rats than in HLM. The enzyme kinetic studies of M1-1 and M1-2 in HLM and in RLM discovered that the formation and further metabolic elimination of both epimers was highly stereoselective, and the stereoselectivity resulted in the metabolism species differences of PPT. In addition, M1-1 and M1-2 were metabolized mainly by CYP3A4 isoform.

Declaration of interest

This work was supported by the National Natural Science Foundation of China (No. 81102880) and the Natural Science Foundation of Shandong Province (No. ZR2012HM036).

References

- Chen G, Yang X, Zhai X, Yang M. (2013). Microbial transformation of 20(S)-protopanaxatriol by *Absidia corymbifera* and their cytotoxic activities against two human prostate cancer cell lines. *Biotechnol Lett* 35:91–5.
- Chiu NT, Guns ES, Adomat H, et al. (2014). Identification of human cytochrome P450 enzymes involved in the hepatic and intestinal biotransformation of 20(S)-protopanaxadiol. *Biopharm Drug Dispos* 35:104–18.
- Evans DC, Baillie TA. (2005). Minimizing the potential for metabolic activation as an integral part of drug design. *Curr Opin Drug Discov Devel* 8:44–50.
- Han B, Meng Q, Li Q, et al. (2011). Effect of 20(S)-protopanaxatriol and its epimeric derivatives on myocardial injury induced by isoproterenol. *Arzneimittelforschung* 61:148–52.
- Han KL, Jung MH, Sohn JH, Hwang JK. (2006). Ginsenoside 20S-protopanaxatriol (PPT) activates peroxisome proliferator-activated receptor gamma (PPARgamma) in 3T3-L1 adipocytes. *Biol Pharm Bull* 29:110–13.
- Hao H, Lai L, Zheng C, et al. (2010). Microsomal cytochrome P450-mediated metabolism of protopanaxatriol ginsenosides: metabolite profile, reaction phenotyping, and structure-metabolism relationship. *Drug Metab Dispos* 38:1731–9.
- Hasegawa E, Nakagawa S, Miyate Y, et al. (2013). Inhibitory effect of protopanaxatriol ginseng metabolite M4 on the production of corticosteroids in ACTH-stimulated bovine adrenal fasciculata cells. *Life Sci* 92:687–93.
- Hasegawa H. (2004). Proof of the mysterious efficacy of ginseng: basic and clinical trials: metabolic activation of ginsenoside: deglycosylation by intestinal bacteria and esterification with fatty acid. *J Pharmacol Sci* 95:153–7.
- Hasegawa H, Sung JH, Matsumiya S, Uchiyama M. (1996). Main ginseng saponin metabolites formed by intestinal bacteria. *Planta Med* 62:453–7.
- Hasegawa H, Suzuki R, Nagaoka T, et al. (2002). Prevention of growth and metastasis of murine melanoma through enhanced natural-killer cytotoxicity by fatty acid-conjugate of protopanaxatriol. *Biol Pharm Bull* 25:861–6.
- He C, Zhou D, Li J, et al. (2014). Identification of 20(S)-protopanaxatriol metabolites in rats by ultra-performance liquid chromatography coupled with electrospray ionization quadrupole time-of-flight tandem mass spectrometry and nuclear magnetic resonance spectroscopy. *J Pharm Biomed Anal* 88:497–508.
- Kasai R, Hara K, Dokan R, et al. (2000). Major metabolites of ginseng saponins formed by rat liver microsomes. *Chem Pharm Bull* 48:1226–7.
- Kong LT, Wang Q, Xiao BX, et al. (2013). Different pharmacokinetics of the two structurally similar dammarane saponins, protopanaxatriol and protopanaxadiol, in rats. *Fitoterapia* 86:48–53.
- Lai L, Hao H, Liu Y, et al. (2009). Characterization of pharmacokinetic profiles and metabolic pathways of 20(S)-ginsenoside Rh1 in vivo and in vitro. *Planta Med* 75:797–802.
- Li L, Chen X, Li D, Zhong D. (2011). Identification of 20(S)-protopanaxadiol metabolites in human liver microsomes and human hepatocytes. *Drug Metab Dispos* 39:472–83.
- Li L, Chen X, Zhou J, Zhong D. (2012). In vitro studies on the oxidative metabolism of 20(s)-ginsenoside Rh2 in human, monkey, dog, rat, and mouse liver microsomes, and human liver S9. *Drug Metab Dispos* 40:2041–53.
- Li XQ, Weidolf L, Simonsson R, Andersson TB. (2005). Enantiomer/enantiomer interactions between the S- and R- isomers of omeprazole in human cytochrome P450 enzymes: major role of CYP2C19 and CYP3A4. *J Pharmacol Exp Ther* 315:777–87.
- Liu L, Gu LJ, Zhang DL, et al. (2010). Microbial conversion of rare ginsenoside Rf to 20(S)-protopanaxatriol by *Aspergillus niger*. *Biosci Biotechnol Biochem* 74:96–100.
- Oh GS, Pae HO, Choi BM, et al. (2004). 20(S)-Protopanaxatriol, one of ginsenoside metabolites, inhibits inducible nitric oxide synthase and

- cyclooxygenase-2 expressions through inactivation of nuclear factor-kappaB in RAW 264.7 macrophages stimulated with lipopolysaccharide. *Cancer Lett* 205:23–9.
- Shibata S. (2001). Chemistry and cancer preventing activities of ginseng saponins and some related triterpenoid compounds. *J Korean Med Sci* 16:28–37.
- Shimshoni JA, Roberts AG, Scian M, et al. (2012). Stereoselective formation and metabolism of 4-hydroxy-retinoic acid enantiomers by cytochrome p450 enzymes. *J Biol Chem* 287:42223–32.
- Sun J, Wang G, Haitang X, et al. (2005). Simultaneous rapid quantification of ginsenoside Rg1 and its secondary glycoside Rh1 and aglycone protopanaxatriol in rat plasma by liquid chromatography-mass spectrometry after solid-phase extraction. *J Pharm Biomed Anal* 38:126–32.
- Sun SY, Wang YQ, Li LP, et al. (2013). Stereoselective interaction between tetrahydropalmatine enantiomers and CYP enzymes in human liver microsomes. *Chirality* 25:1:43–7.
- Tawab MA, Bahr U, Karas M, et al. (2003). Degradation of ginsenosides in humans after oral administration. *Drug Metab Dispos* 31:1065–71.
- Tian Y, Guo H, Han J, Guo D. (2005). Microbial transformation of 20(S)-protopanaxatriol by *Mucor spinosus*. *J Nat Prod* 68:678–80.
- Usami Y, Liu YN, Lin AS, et al. (2008). Antitumor agents. 261. 20(S)-protopanaxadiol and 20(s)-protopanaxatriol as antiangiogenic agents and total assignment of (1)H NMR spectra. *J Nat Prod* 71:478–81.
- Wang YZ, Chen J, Chu SF, et al. (2009). Improvement of memory in mice and increase of hippocampal excitability in rats by ginsenoside Rg1's metabolites ginsenoside Rh1 and protopanaxatriol. *J Pharmacol Sci* 109:504–10.
- Wang YZ, Wang YS, Chu SF, et al. (2010). Protopanaxatriol metabolites identified by LC-MS/MS after oral administration in mice. *Int J Clin Pharmacol Ther* 48:282–90.
- Zhang J, Guo H, Tian Y, et al. (2007). Biotransformation of 20(S)-protopanaxatriol by *Mucor spinosus* and the cytotoxic structure activity relationships of the transformed products. *Phytochemistry* 68:2523–30.